Nuclear Inst. and Methods in Physics Research, A 866 (2017) 252–264

Contents lists available at ScienceDirect

Nuclear Inst. and Methods in Physics Research, A

journal homepage: www.elsevier.com/locate/nima

Real-time neutron source localization and identification with a hand-held, volumetrically-sensitive, moderating-type neutron spectrometer

C.B. Hoshor [a], E.R. Myers [a], T.M. Oakes [b,c], S.M. Young [a], J.E. Currie [a,e], P.R. Scott [a,e], W.H. Miller [c,d], S.L. Bellinger [f,g], D.S. McGregor [f], A.N. Caruso [a,*]

[a] Department of Physics, University of Missouri — Kansas City, Kansas City, MO, United States
[b] Sandia National Laboratories, National Nuclear Security Administration's Kansas City National Security Campus, Kansas City, MO, United States
[c] Nuclear Science and Engineering Institute, University of Missouri – Columbia, Columbia, MO, United States
[d] Missouri University Research Reactor, Columbia, MO, United States
[e] U2D Incorporated, Kansas City, MO, United States
[f] Department of Mechanical and Nuclear Engineering, Kansas State University, Manhattan, KS, United States
[g] Radiation Detection Technologies, Manhattan, KS, United States

ARTICLE INFO

Keywords:
Neutron spectrometer
Solid-state neutron detector
Neutron source identification
Neutron source localization
Portable neutron detector
Moderating spectrometer

ABSTRACT

Measuring source-dependent properties of free neutrons over a large neutron energy range, with hand-portable instrumentation, continues to push the frontier of neutron detection instrumentation design and analysis techniques. Building on prior work – C.B. Hoshor, et al., A portable and wide energy range semiconductor-based neutron spectrometer, Nucl. Instrum. Methods Phys. Res. A 803 (2015) 68–81 – which focused on demonstrating one-dimensional-based energy-dependent neutron measurement and analysis with a new class of solid-state moderating-type spectrometer, this work introduces two "core" algorithmic methodologies that expand the analysis of neutron thermalization measurements to three spatial dimensions to determine the location and identity of neutron radiation sources in real time. Two extensions of these core methodologies are then proposed to further improve both the accuracy and reliability of source location and identity determinations with this new class of hand-held instrumentation. In 432 preliminary simulation tests, these method extensions are shown to decrease the average source location error by 64% and provide correct identity determinations in all test cases.

1. Introduction

1.1. Background and motivation

Hand-held instruments that passively detect, locate, and identify unknown sources of neutron radiation – either bare or obscured (i.e. shielded) by neutron moderating and/or absorbing material(s) – in real time, are important to nuclear non-proliferation applications. This application space requires real-time energy-sensitive measurement of free neutrons, ranging from thermal energies (~25 meV) to the top end of the evaporation spectrum (~20 MeV). To this end, the first representatives of a new class of solid-state moderating-type neutron spectrometer [1] have been iteratively designed to improve on multi-sphere- [2,3] and long-counter-based [4] moderating-type neutron spectrometers (see [1,5], and references therein, for information on prior art and history of development). Improvements include reduced instrument mass, greater detection efficiency than the present art, and real-time analysis of energy-sensitive neutron thermalization measurements in three spatial dimensions. It is the unique, energy-sensitive, three-dimensional neutron thermalization information afforded by this new class of instruments (introduced in [1]), coupled with the analysis techniques discussed herein, that is novel, and will be the primary focus of this work.

1.2. The 6C hand-held solid-state neutron spectrometer

Although the general methodologies introduced in this work could be applied to a wide variety of similar instrument designs, the discussion herein will primarily focus on the research team's most successful instrument to date, the 6C (6-inch Cylindrical) moderating-type neutron

* Correspondence to: 257 Flarsheim Hall, 5110 Rockhill Road, Kansas City, MO 64110, United States.
E-mail address: carusoan@umkc.edu (A.N. Caruso).

http://dx.doi.org/10.1016/j.nima.2017.05.033
Received 18 April 2017; Received in revised form 20 May 2017; Accepted 22 May 2017
Available online 10 July 2017
0168-9002/

spectrometer. This section will provide a brief description of the 6C neutron spectrometer and the unique neutron thermalization information afforded by the instrument.

The active portion of the 6C neutron spectrometer, as shown in Fig. 1.1(C), consists of 8 neutron detector daughter boards evenly-spaced (axially) within a cylindrical volume (diameter = 6″, length = 12″) of high density polyethylene (HDPE) moderator. Each of the 8 detector daughter boards (Fig. 1.1(A)) is composed of a 4 × 4 square array of 2.0-cm × 2.0-cm microstructured neutron detectors (MSNDs). The MSND-based boards, developed and manufactured by Radiation Detection Technologies (RDT), are comprised of Si diodes, etched to form trenches and backfilled with ^{6}LiF powder; the MSND variant used in this work has an empirical thermal neutron detection efficiency of $\eta_{\text{th}} \approx 22\%$ (the MSND detection mechanism has been described in detail previously [6]).

The fundamental novelty of the 6C spectrometer's design is that the internal array of 128 thin (≈525 μm), semiconductor-based, thermal neutron detectors (MSNDs) provides high neutron detection efficiency and volumetric resolution of the average neutron thermalization along three coordinate axes within the moderator–detector assembly, with minimal displacement of the moderating medium. The primary goal of this work is to introduce novel algorithmic methodologies that utilize this highly-efficient, statistically-predictable, three-dimensional neutron thermalization information (see Fig. 1.2) to determine the relative location and the identity of neutron radiation sources in real time. Sections 2 and 3 of this paper will introduce and discuss the "core" methods (currently implemented in the 6C spectrometer software) for determining the relative location and the identity of neutron sources. Sections 4 and 5 will then explore extensions of – and potential improvements to – these core methodologies.

2. Neutron response vectorization (NRV) method for determining neutron source location

2.1. NRV method description

The simulations represented in Fig. 1.2 illustrate the statistically-predictable dependence of the 6C spectrometer response (i.e., MSND detection intensities as a function of location within the moderating medium) with respect to the relative angular position of a neutron source of interest in the horizontal plane. Utilizing this dependence, the currently implemented algorithm for determining the location of a neutron source (relative to the 6C spectrometer) employs a 3-dimensional vector-summing method called the neutron response vectorization (NRV) method (note: the discussion in this section will be in terms of the common coordinate system defined in Figs. 1.2(A) and 2.1(A) unless otherwise specified). In the first step of this method, each neutron detector in the instrument is assigned a vector, $\boldsymbol{r}_l$, describing its physical location relative to the midpoint of the moderating medium's central axis (Fig. 2.1(B)),

$$\boldsymbol{r}_l = \begin{bmatrix} x_l \\ y_l \\ z_l \end{bmatrix}, \quad \text{for } l = 1, \ldots, Q, \tag{2.1}$$

where Q is the total number of detectors in the system (for the 6C spectrometer, $Q = 128$). Next, geometric corrections are made to account for instrument asymmetries. By way of example, in the case of the 6C spectrometer, since the internal MSND arrays form a rectangular-prism-shaped grid within the moderator volume (as shown in Fig. 1.2), the currently-implemented NRV algorithm for this instrument employs a vector of Cartesian geometric expansion coefficients, $\Lambda = [\lambda_x, \lambda_y, \lambda_z]^T$, to multiplicatively transform the position vectors, $\boldsymbol{r}_l = [x_l, y_l, z_l]$, from their original rectangular prism orientation, to an expanded cubic form (Fig. 2.1(C)). This transformation is given by

$$\boldsymbol{c}_l \equiv r_l \circ \Lambda = \begin{bmatrix} \boldsymbol{x_l} \cdot \lambda_x \\ \boldsymbol{y_l} \cdot \lambda_y \\ \boldsymbol{z_l} \cdot \lambda_z \end{bmatrix}, \quad \text{where} \tag{2.2}$$

$$\lambda_x = 1, \qquad \lambda_y = \frac{\max(x_l) - \min(x_l)}{\max(y_l) - \min(y_l)}, \quad \text{and} \quad \lambda_z = \frac{\max(x_l) - \min(x_l)}{\max(z_l) - \min(z_l)},$$

(the operator "∘" represents the Hadamard product, i.e., element-wise multiplication). These cubic-oriented position vectors are then normalized to form spherically-oriented unit vectors (Fig. 2.1(D)),

$$\boldsymbol{u}_l \equiv \frac{\boldsymbol{c}_l}{|\boldsymbol{c}_l|} = \frac{\boldsymbol{r}_l \circ \Lambda}{|\boldsymbol{r}_l \circ \Lambda|} = \frac{1}{\sqrt{(x_l \cdot \lambda_x)^2 + (y_l \cdot \lambda_y)^2 + (z_l \cdot \lambda_z)^2}} \cdot \begin{bmatrix} x_l \cdot \lambda_x \\ y_l \cdot \lambda_y \\ z_l \cdot \lambda_z \end{bmatrix}. \tag{2.3}$$

Since these vectors are oriented spherically, they possess the highest degree of rotational symmetry achievable for the discrete system (i.e., Q discrete unit vectors, $\boldsymbol{u}_l$, $l = 1, \ldots, Q$). With geometric asymmetries aptly accounted for and each position vector normalized, the number of neutron counts registered by each detector, N_l, is then multiplied by its associated unit vector, $\boldsymbol{u}_l$, yielding a set of detector response vectors (Fig. 2.1(E))

$$\begin{aligned} \boldsymbol{d}_l &\equiv N_l \cdot \boldsymbol{u}_l = N_l \cdot \frac{\boldsymbol{r}_l \circ \Lambda}{|\boldsymbol{r}_l \circ \Lambda|} \\ &= \frac{N_l}{\sqrt{(x_l \cdot \lambda_x)^2 + (y_l \cdot \lambda_y)^2 + (z_l \cdot \lambda_z)^2}} \cdot \begin{bmatrix} x_l \cdot \lambda_x \\ y_l \cdot \lambda_y \\ z_l \cdot \lambda_z \end{bmatrix}. \end{aligned} \tag{2.4}$$

All Q detector response vectors are then summed, resulting in a single resultant vector (Fig. 2.1(F)),

$$\begin{aligned} \boldsymbol{v}^{(R)} &\equiv \sum_{l=1}^{Q} \boldsymbol{d}_l = \sum_{l=1}^{Q} N_l \cdot \frac{\boldsymbol{r}_l \circ \Lambda}{|\boldsymbol{r}_l \circ \Lambda|} \\ &= \sum_{l=1}^{Q} \frac{N_l}{\sqrt{(x_l \cdot \lambda_x)^2 + (y_l \cdot \lambda_y)^2 + (z_l \cdot \lambda_z)^2}} \cdot \begin{bmatrix} x_l \cdot \lambda_x \\ y_l \cdot \lambda_y \\ z_l \cdot \lambda_z \end{bmatrix}. \end{aligned} \tag{2.5}$$

Since this equation is expressed in terms of each detector's physical position, r_l (predetermined/constant), and number of counts registered, N_l (measured/variable), with geometric expansion coefficients, Λ (predetermined/constant) as defined in Eq. (2.2), this resultant vector can be calculated from Eq. (2.5), alone, as the measured data accumulates (i.e., in real time). The direction of the resultant vector, $\boldsymbol{v}^{(R)}$, indicates the region of the instrument with the highest average detection intensity, and its magnitude is proportional to the degree of spatial localization (or dispersion) of this high intensity region. It is important to note here that both the direction and magnitude of $\boldsymbol{v}^{(R)}$ are altered, to some degree, with the introduction of any geometric asymmetry corrections, and this must be carefully considered in light of an instrument's design. However, in the case of the 6C spectrometer, the correction step described in Eq. (2.2) has been shown to improve the accuracy of this method – in comparison to skipping this step – regardless of source-to-spectrometer relative angular orientation, and has thus been incorporated into the core NRV methodology described here, by way of example. This vector, $\boldsymbol{v}^{(R)}$, is then normalized to produce a resultant unit vector, $\boldsymbol{u}^{(R)}$, in the expected direction of the neutron source of interest (Fig. 2.1(G)),

$$\boldsymbol{u}^{(R)} \equiv \frac{\boldsymbol{v}^{(R)}}{|\boldsymbol{v}^{(R)}|} = \frac{1}{\sqrt{\left(v_x^{(R)}\right)^2 + \left(v_y^{(R)}\right)^2 + \left(v_z^{(R)}\right)^2}} \cdot \begin{bmatrix} v_x^{(R)} \\ v_y^{(R)} \\ v_z^{(R)} \end{bmatrix}. \tag{2.6}$$

Fig. 2.1(B)–(D), provides a step-by-step visualization of the six major steps of the NRV method. For the example shown in Fig. 2.1, the NRV method was applied to a simulated 6C spectrometer response to a bare ^{252}Cf point source 2 m from what will be defined here as the moderating cylinder's circular "front face", located at $x = -12.6$ cm in Figs. 1.2(A) and 2.1(A) (i.e., the leftmost circular face in Fig. 1.1(B)–(D)). Notes: (1) Figs. 1.2(A) and 2.1(A) depict same simulated response data, (2) the ^{252}Cf energy spectrum used in this simulation is a "measured" spectrum

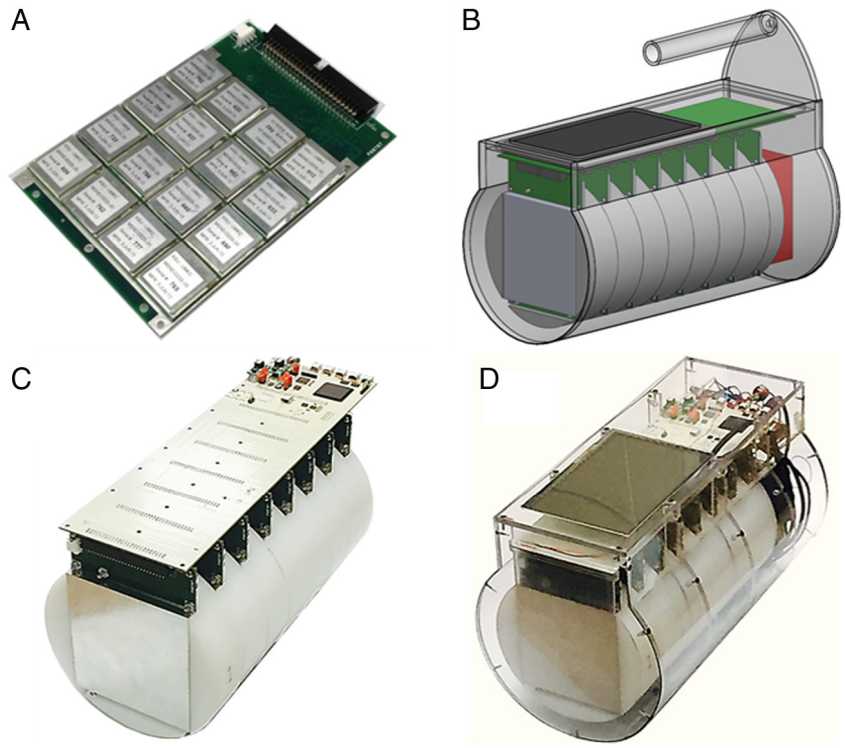

Fig. 1.1. Photographs and renderings of a prototype 6C system; showing (A) an individual printed circuit board with mounted microstructured neutron detectors, (B) assembly view showing the 8 boards within the moderator volume (composed of 8 recessed HDPE slabs), motherboard, capacitive touch screen display, Li-ion battery pack, and transparent polycarbonate case (CPU not displayed), (C) assembled instrument with the case, touch screen display, battery pack, and CPU removed, and (D) fully assembled 6C neutron spectrometer (handle removed).

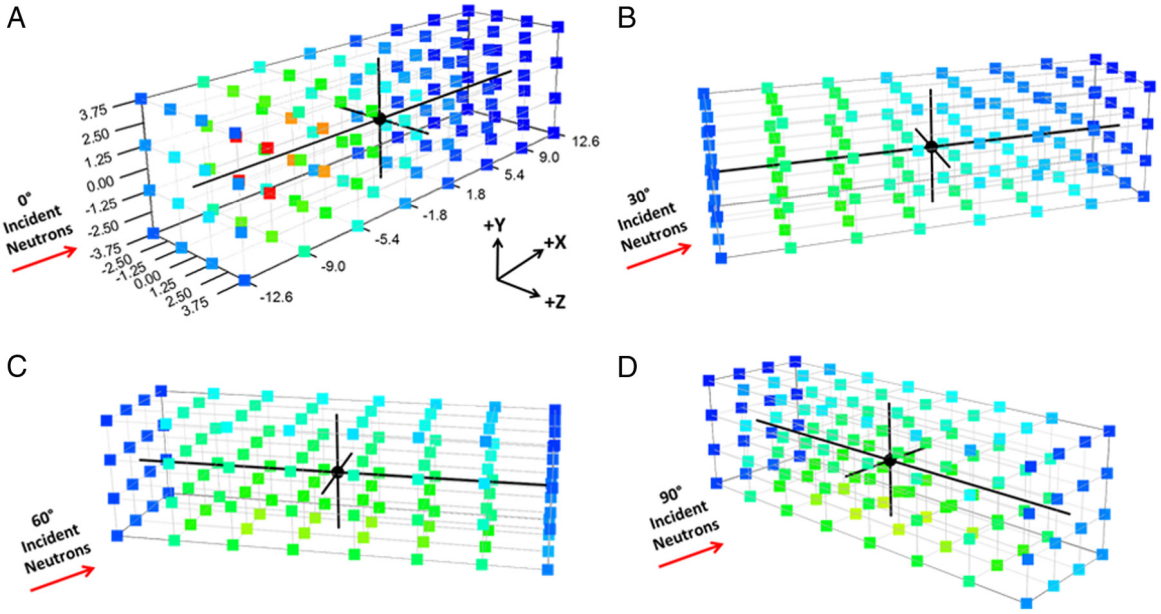

Fig. 1.2. Simulated examples of 6C spectrometer responses – relative MSND detection intensities (color scale) as a function of (x, y, z) position (in cm, coordinate system shown in Figure A) within the cylindrical moderator volume – to a bare ^{252}Cf spontaneous fission neutron source [7,8] at a standoff distance of 2 m; showing relative source-to-spectrometer angular orientations of (A) 0°, (B) 30°, (C) 60°, and (D) 90°. Common color scale: highest detection intensity = Red → lowest detection intensity = Dark Blue, normalized to Figure A. (For interpretation of the references to color in this figure legend, the reader is referred to the web version of this article.)

(specifically, an unfolded spectrum from Bonner sphere spectrometer measurements, in which the shadow cone method was employed to eliminate environmental scatter contributions; [7,8]), (3) in the common coordinate system shown in these figures, the position of the ^{252}Cf point source was [−212.6 cm, 0 cm, 0 cm], (4) no environmental factors, other than the presence of air, were included in this simulation (i.e., no floor/ground, ceiling, walls, objects, etc. were simulated), (5) in total, 90594 neutrons were detected by the instrument in this simulation.

The resultant unit vector obtained through application of the NRV method to this simulated 6C spectrometer response (shown in Fig. 2.1(G)) is $\boldsymbol{u}^{(R)} \cong [-0.999994, -0.001653, -0.003025]$, extremely close to the true (normalized) source direction, [−1, 0, 0], in this idealized case (i.e., no environment simulated). However, in most real-world

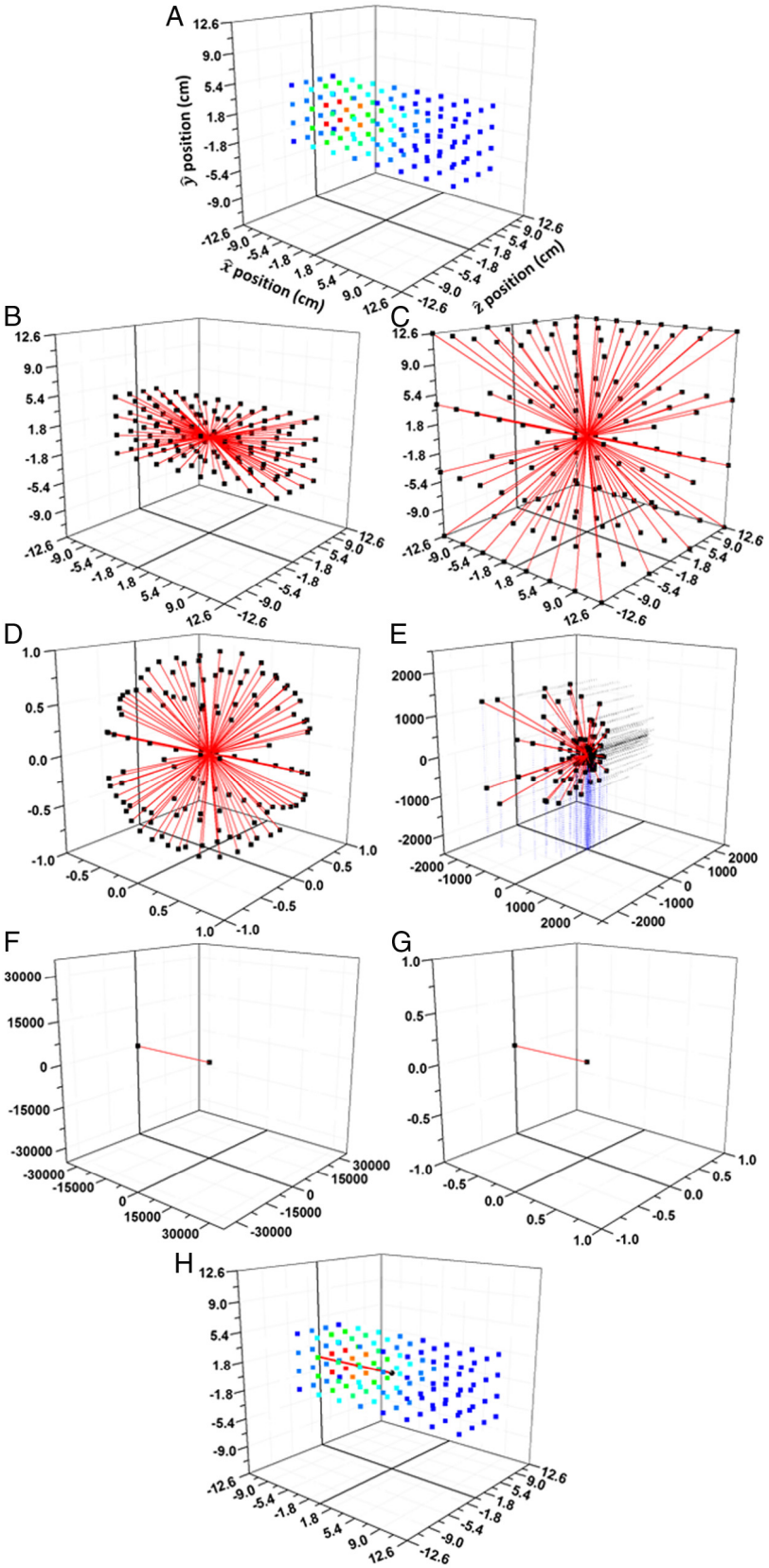

Fig. 2.1. (A) Simulated 6C spectrometer response to a bare ^{252}Cf point source located at [−212.6, 0, 0] in the defined coordinate system (axis labels common in Figures A–H). Step-by-step visualization of the NRV method, applied to (A); showing (B) initial detector position vectors $\boldsymbol{r}_l$ (Eq. (2.1)), (C) post-asymmetry-correction cubic-oriented position vectors $\boldsymbol{c}_l$ (Eq. (2.2)), (D) post-normalization spherically-oriented unit vectors $\boldsymbol{u}_l$ (Eq. (2.3)), (E) detector response vectors $\boldsymbol{d}_l$ (Eq. (2.4); dotted projection lines added for visual clarity), (F) summed resultant vector $\boldsymbol{v}^{(R)}$ (Eq. (2.5)) with magnitude proportional to the degree of spatial response localization (or dispersion), and (G) resultant unit vector $\boldsymbol{u}^{(R)}$ (Eq. (2.6)) in the suspected direction of the neutron source. (H) NRV method result shown in context of Figure A.

environments, when an empirical measurement is taken in this source-to-spectrometer angular orientation, a small but non-negligible portion of the detected neutrons will undergo scattering interactions (and resultant energy loss) from the ground before entering the instrument volume (note: other sources of room return are discussed below), creating a vertical asymmetry in the instrument response. This response asymmetry results in a false and non-negligible $\boldsymbol{u}^{(R)}$ vector component in the $-\hat{z}$ direction (i.e., downward; typically between $-1°$ and $-10°$ from the horizontal plane, depending upon environmental conditions). The fact that this $\hat{z}$ component is not indicative of the true source position, highlights the primary shortcoming of the NRV method (see [9] for additional information and examples). From measurements amassed on the 6C spectrometer, the instrument's response in the vertical dimension has empirically proven to be much more sensitive to variations in environmental scattering conditions than its horizontal-planar response components (i.e., the instrument's response is more sensitive to ground scatter than other sources of room return, e.g., walls, ceilings, objects, etc.). Hence, predicting the relative location of a neutron source in the vertical dimension from 6C spectrometer measurements represents a particularly challenging problem, and is outside the scope of this first work regarding the NRV method; solutions will be addressed in future work.

In light of these inherent difficulties regarding vertical angular resolution, the remainder of this work regarding neutron source localization will primarily focus on determining the angular location in the horizontal plane. To do so using the NRV method, consider the projection of the vector $\boldsymbol{v}^{(R)}$ (as defined previously, Eq. (2.5)) onto the horizontal x–z-plane. Formally, this projection is given by

$$\boldsymbol{v}^{(H)} \equiv \boldsymbol{v}^{(R)} - \left(\boldsymbol{v}^{(R)} \cdot \boldsymbol{n}\right)\boldsymbol{n},$$

where $\boldsymbol{v}^{(R)} = \begin{bmatrix} v_x^{(R)} \\ v_y^{(R)} \\ v_z^{(R)} \end{bmatrix}$ (from Eq. (2.5)), and $\boldsymbol{n} = \begin{bmatrix} 0 \\ 1 \\ 0 \end{bmatrix}$ (unit vector normal to the x–z-plane), such that

$$\begin{aligned} \boldsymbol{v}^{(H)} &\equiv \begin{bmatrix} v_x^{(R)} \\ v_y^{(R)} \\ v_z^{(R)} \end{bmatrix} - \left(\begin{bmatrix} v_x^{(R)} & v_y^{(R)} & v_z^{(R)} \end{bmatrix} \begin{bmatrix} 0 \\ 1 \\ 0 \end{bmatrix} \right) \begin{bmatrix} 0 \\ 1 \\ 0 \end{bmatrix} \\ &= \begin{bmatrix} v_x^{(R)} \\ v_y^{(R)} \\ v_z^{(R)} \end{bmatrix} - v_y^{(R)} \cdot \begin{bmatrix} 0 \\ 1 \\ 0 \end{bmatrix} \Longrightarrow \boldsymbol{v}^{(H)} \equiv \begin{bmatrix} v_x^{(R)} \\ 0 \\ v_z^{(R)} \end{bmatrix}. \end{aligned} \tag{2.7}$$

Thus, normalization of $\boldsymbol{v}^{(H)}$ yields the resultant unit vector,

$$\boldsymbol{u}^{(H)} \equiv \frac{\boldsymbol{v}^{(H)}}{\left|\boldsymbol{v}^{(H)}\right|} = \frac{1}{\sqrt{\left(v_x^{(R)}\right)^2 + 0^2 + \left(v_z^{(R)}\right)^2}} \cdot \begin{bmatrix} v_x^{(R)} \\ 0 \\ v_z^{(R)} \end{bmatrix}, \tag{2.8}$$

in the expected direction of the neutron source in the horizontal plane. Note: due to our choice of coordinate system, this projection is equivalent to ignoring the vertical component.

With $\boldsymbol{u}^{(H)}$ determined, providing a vector description of the expected neutron source location in the horizontal plane, it is now possible to provide a corresponding angular description. The relative source-to-spectrometer angular orientation in the horizontal x–z-plane, θ, will be defined in this work as the angle (measured counterclockwise) between a unit vector in the $-\hat{x}$ direction, $[-1, 0, 0]^T$ (toward the front face of the instrument), and the vector position of the neutron source of interest, projected onto the horizontal plane, $\left[x_{source}, 0, z_{source}\right]^T$. Following this definition, the relative source-to-spectrometer angular orientation in the horizontal x–z-plane, as predicted by the NRV method, θ_{NRV}, may then be calculated as the angle (measured counterclockwise) between $[-1, 0, 0]^T$ and $\boldsymbol{u}^{(H)} = \left[u_x^{(H)}, u_y^{(H)}, u_z^{(H)}\right]^T$. Eq. (2.9), below, shows how θ_{NRV} (in radians) is calculated in the 6C spectrometer software, conditional upon the values of the x- and z-axial components of $\boldsymbol{u}^{(H)}$ obtained from Eq. (2.8) ($u_y^{(H)} = 0$).

$$\theta_{\mathrm{NRV}} = \begin{cases} \tan^{-1}\left|\dfrac{u_z^{(H)}}{u_x^{(H)}}\right|; & u_x^{(H)} < 0,\ u_z^{(H)} \geq 0 \\ \pi - \tan^{-1}\left|\dfrac{u_z^{(H)}}{u_x^{(H)}}\right|; & u_x^{(H)} > 0,\ u_z^{(H)} \geq 0 \\ \pi + \tan^{-1}\left|\dfrac{u_z^{(H)}}{u_x^{(H)}}\right|; & u_x^{(H)} > 0,\ u_z^{(H)} < 0 \\ 2\pi - \tan^{-1}\left|\dfrac{u_z^{(H)}}{u_x^{(H)}}\right|; & u_x^{(H)} < 0,\ u_z^{(H)} < 0 \\ \dfrac{\pi}{4}; & u_x^{(H)} = 0,\ u_z^{(H)} < 0 \\ \dfrac{3\pi}{4}; & u_x^{(H)} = 0,\ u_z^{(H)} > 0 \\ undefined; & u_x^{(H)} = 0,\ u_z^{(H)} = 0. \end{cases} \tag{2.9}$$

2.2. 6C software implementation

As currently implemented in the 6C spectrometer software, the resultant unit vector, $\boldsymbol{u}^{(H)}$, is displayed graphically – as an arrow indicating the suspected direction of the neutron source of interest – and the angular orientation, θ, is displayed numerically on the source location screen of the instrument's graphical user interface (GUI) for both static (stationary source and stationary instrument) and dynamic (moving source and/or moving instrument) modes of operation, updating in real time.

2.3. Empirical analysis of NRV method

2.3.1. Experimental setup

To empirically test the efficacy of the NRV method with the 6C spectrometer, studies were conducted indoors, in the center of a 20-ft. × 30-ft. × 11-ft. (height) room with concrete walls and floor (i.e., a high neutron scattering environment, chosen to represent challenging conditions for the NRV method), in which spectrometer measurements were taken at a 2.0-m standoff distance from a bare 1.5×10^5-n/s ^{252}Cf source, at relative angular orientations ranging from 0° to 180° in +10° increments (19 empirical measurements total). Each measurement was terminated once a cumulative count total of 3000 was exceeded for counting-statistical certainty and consistency of results (3000 total counts corresponds to a 95% confidence interval of approximately ±0.05° using standard error propagation). Measurements were also taken from 180° to 360°, but these are not shown in the figure because the results from 360° to 180° in −10° increments were nearly identical to the results from 0° to 180° in +10° increments due to instrument symmetry.

2.3.2. Empirical results

The results of these empirical tests (Fig. 2.2) show that the NRV method, applied to 6C spectrometer measurements, provided an accurate determination of the relative horizontal-planar angular location of the neutron source, in a high-scattering environment, with an average angular error of ±7° (i.e., $(1/n) \cdot \sum_{i=1}^{n} \left|\theta^{(i)} - \theta_{\mathrm{NRV}}^{(i)}\right| = 7°$, with $i = 1, \ldots, n$ enumerating the empirical tests conducted). Although this average angular error may be acceptable for many applications, a major goal for this current work (as well as future methodological developments) is to reduce the average error as much as possible, while also improving error consistency for all source-spectrometer angular orientations (e.g., "measured angles", using the NRV method, are *consistently* less accurate for "true angles" of 20°–30° and 100°–110° than those for true angles of 70°–80° and 160°–170°, which is not desirable).

It is important to note here that the apparent trend in the results of Fig. 2.2 (from 0° to 90° and repeating from 90° to 180°) is not simply a statistical anomaly, nor is it due to systematic measurement

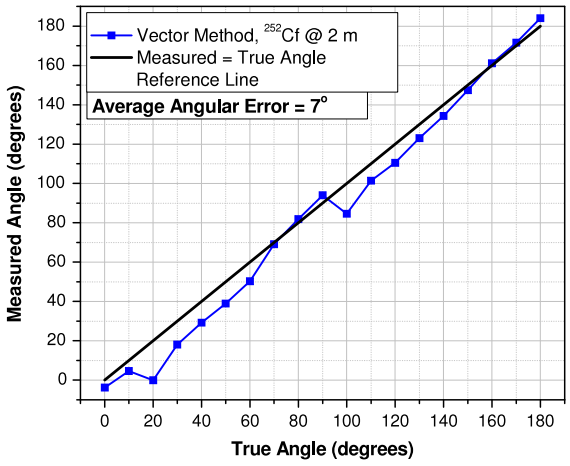

Fig. 2.2. Summary plot of 6C empirical test results for determining source-to-spectrometer angular orientation in the horizontal plane using the NRV method; showing instrument measurements from a bare 1.5×10^5-n/s ^{252}Cf spontaneous fission neutron source at a 2.0-m standoff distance. Measured angle = true angle line (solid black line) included for reference.

error; this general trend is a direct consequence of the 6C spectrometer's cylindrical geometry (which is asymmetric in the horizontal x–z-plane) in combination with the applied NRV method. The consistency of this observed trend indicates that further geometric-asymmetry corrections can be applied to the NRV method, which could potentially decrease the average angular error for the 6C spectrometer. One such potential algorithmic improvement will be discussed in Section 5. Having now introduced the core methodology used for determining source location based on 6C spectrometer measurements, the next section will discuss the core methodologies utilized to determine the identity of a neutron source, and the way in which these methods are algorithmically implemented.

3. Pearson product-moment cross-correlation spatial response analysis techniques for neutron source identification

3.1. Pearson cross-correlation method description

The primary goal of the Pearson product-moment cross-correlation methodologies discussed in this section is to determine the most probable identity of a neutron source, based upon moderating-type spectrometer measurements, by exploiting the probabilistic – and therefore statistically predictable – nature of neutron scattering and thermalization in a hydrogenous moderating medium. To this end, these methods employ correlation-based template-matching procedures to analyze the response of a volumetrically-sensitive spectrometer in one 1, 2, and/or 3 spatial dimensions, in relationship to a "library" of a priori information (i.e., a database of pertinent information that is knowable prior to measurement). Although this underlying concept could be applied to volumetrically-sensitive moderating-type instruments of nearly any conceivable design, many aspects of such algorithms can potentially be (and, in most cases, *should* be) specifically catered to the geometry of a particular instrument. The remainder of this section will focus on the methods developed specifically for the 6C spectrometer.

For a moderating-type instrument that is inherently invariant to source-to-instrument relative angular orientation (e.g., an idealized Bonner sphere spectrometer, BSS; [2,3]), techniques such as those described in this section may be applied in a direct manner; however, for angular-orientation-dependent instruments (e.g., the 6C spectrometer), a reference orientation must be defined prior to application of the spatial response analysis methodologies described herein. For the 6C spectrometer, this reference orientation was chosen such that the instrument's front circular face is directed toward the neutron source of interest; and operationally, the user is required – while in "source identification mode" – to reorient the instrument to this reference orientation prior to beginning a source identification data collection. If the user is unaware of the location of a neutron source, the instrument software currently provides a separate "source search mode", in which the NRV method (discussed in Section 2) is employed to estimate the location of the source (relative to the instrument) and display this information to the user. Additionally, prior to the application of these spatial response analysis methods, a library of expected or known spectrometer responses must be uploaded to the instrument's software. These responses, referred to here as "library responses", are generated through either MCNP simulation or empirical measurement – such that the front circular face of the instrument is oriented toward the neutron source – to include as many neutron source types and shielded variants as necessary for a given application (e.g., a reasonably extensive library, pre-generated by the research team, is included in the instrument's software). Alternatively, a priori source information may be uploaded in the form of neutron energy spectra. In this case, the energy spectra must be normalized, rebinned, and folded into (i.e., multiplied by) the instrument's response matrix (pre-loaded in the 6C software, for front-face orientation) to generate expected response libraries for the new source type(s). Once all neutron sources of interest are accounted for in the library, the responses are grouped for 1-, 2-, and/or 3-dimensional analysis (discussed in Sections 3.1.1, 3.1.2, and 3.1.3, respectively). With the proper response libraries uploaded and grouped, and the front face of the spectrometer oriented in the suspected direction of the neutron source of interest, the user may start the data collection for neutron source identification. During data collection, the live response data is grouped for 1-, 2-, and/or 3-dimensional real-time comparison to each individual library response using the Pearson product-moment cross-correlation coefficient [10], given by

$$r_{\boldsymbol{A},\boldsymbol{B}} = \frac{1}{n} \cdot \sum_{i=1}^{n} \frac{A_i - \bar{A}}{\sigma_{\boldsymbol{A}}} \cdot \frac{B_i - \bar{B}}{\sigma_{\boldsymbol{B}}}, \tag{3.1}$$

where n is the number of response groupings, $\boldsymbol{A} = \left[A_1, A_2, \ldots, A_n\right]^T$ represents the live collection response data set, $\boldsymbol{B} = \left[B_1, B_2, \ldots, B_n\right]^T$ represents one library response data set, and $\bar{A}$, $\bar{B}$, $\sigma_{\boldsymbol{A}}$, and $\sigma_{\boldsymbol{B}}$ represent the averages and standard deviations of response data sets $\boldsymbol{A}$ and $\boldsymbol{B}$ respectfully. This coefficient results in a value in the range [−1, 1] which is a measure of linear correlation (similarity) between the live instrument response, $\boldsymbol{A}$, and a particular library response, $\boldsymbol{B}$, where $r_{\boldsymbol{A},\boldsymbol{B}} = 1$ indicates a total positive correlation (the responses are exactly the same), $r_{\boldsymbol{A},\boldsymbol{B}} = 0$ indicates no correlation (the responses are entirely different), and $r_{\boldsymbol{A},\boldsymbol{B}} = -1$ indicates a total negative correlation (the responses are exactly opposite). The square of this correlation coefficient, $r^2_{\boldsymbol{A},\boldsymbol{B}}$, called the coefficient of determination, results in a value in the range [0, 1] which represents the magnitude of linear correlation (similarity) between the two responses. The single library response that is most positively correlated to the live response, according to the value of $r^2_{\boldsymbol{A},\boldsymbol{B}}$, is then chosen as the most likely source of the incident neutron radiation (of the libraries uploaded). Note: the occurrence of a negative correlation is extremely rare in this application; however, if a correlation, $r_{\boldsymbol{A},\boldsymbol{B}}$, happens to be negative, the magnitude of correlation is calculated as $-\left(r^2_{\boldsymbol{A},\boldsymbol{B}}\right)$, in order to avoid the misidentification of a negatively correlated response data set.

3.1.1. 1-Dimensional spectrometer response analysis

For the 1-dimensional response analysis, the counts from all 16 MSNDs are summed for each of the 8 detector daughter boards, providing the spectrometer response as a function of axial depth (Fig. 3.1), with each of the 8 data points given by

$$N\left(x_i\right) = \sum_{k=1}^{n_z} \sum_{j=1}^{n_y} N\left(x_i, y_j, z_k\right), \quad \text{for } i = 1, \ldots, n_x, \tag{3.2}$$

where n_x, n_y, and n_z are the number of unique x- y- and z-axial detector positions, respectively (for the 6C spectrometer, $n_x = 8$ and $n_y = n_z = 4$).

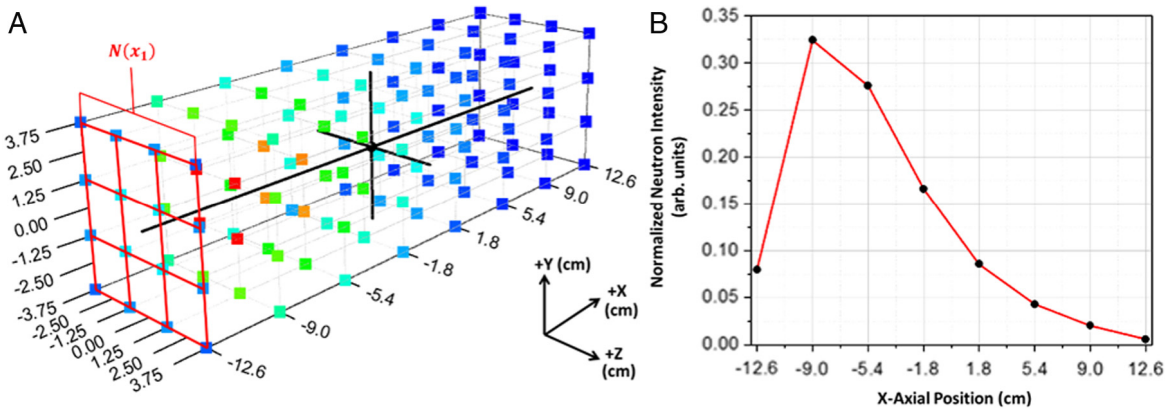

Fig. 3.1. (A) Example of a 1-dimensional cross-correlation data grouping applied to a simulated 6C spectrometer response to a bare ^{252}Cf neutron source, showing the x-axial grouping for MSNDs located at $x_1 = -12.6$ cm in the defined 3-dimensional coordinate system. (B) Linear plot of the grouped 1-dimensional spectrometer response, showing normalized neutron detection intensity (arbitrary units) as a function of x-axial position (in cm) in the coordinate system defined in Figure A, resulting from application of Eq. (3.2) (black circles with red linear interpolation lines). (For interpretation of the references to color in this figure legend, the reader is referred to the web version of this article.)

In this case, the Pearson product-moment cross-correlation coefficient takes the form

$$r_{C,L} = \frac{1}{n_x} \cdot \sum_{i=1}^{n_x} \frac{N_C\left(x_i\right) - \overline{N_C\left(x\right)}}{\sigma_{\boldsymbol{N}_C(x)}} \cdot \frac{N_L\left(x_i\right) - \overline{N_L\left(x\right)}}{\sigma_{\boldsymbol{N}_L(x)}}, \tag{3.3}$$

where $\boldsymbol{N}_C(x) = [N_C(x_1), \ldots, N_C(x_{n_x})]^T$ represents the collection response and $\boldsymbol{N}_L(x) = [N_L(x_1), \ldots, N_L(x_{n_x})]^T$ represents one library response.

3.1.2. 2-dimensional spectrometer response analysis

Noting that the spectrometer responses appear to be radially symmetric about the central x-axis (see Fig. 3.1(A)), it may be beneficial to extend our analysis to include the response's radial dependence. For this 2-dimensional response analysis, the MSND counts are summed according to both their axial position and radial distance from the cylindrical moderating medium's central axis (three possible radii, Fig. 3.2(A)) in cylindrical coordinates. This data grouping provides the spectrometer response as a function of both radius and axial depth, with each of the 24 data points ($n_\theta = 12$, $n_r = 3$, and $n_x = 8 \Rightarrow n_r \cdot n_x = 3 \cdot 8$) given by

$$N\left(r_i, x_j\right) = \sum_{k=1}^{n_\theta} N\left(r_i, x_j, \theta_k\right), \quad \text{for } i = 1, \ldots, n_r;\ j = 1, \ldots, n_x. \tag{3.4}$$

In this case, the Pearson product-moment cross-correlation coefficient takes the form

$$r_{C,L} = \frac{1}{n_r \cdot n_x} \cdot \sum_{j=1}^{n_x} \sum_{i=1}^{n_r} \frac{N_C\left(r_i, x_j\right) - \overline{\boldsymbol{N}_C\left(r, x\right)}}{\sigma_{\boldsymbol{N}_C(r,x)}} \cdot \frac{N_L\left(r_i, x_j\right) - \overline{\boldsymbol{N}_L\left(r, x\right)}}{\sigma_{\boldsymbol{N}_L(r,x)}}, \tag{3.5}$$

where $\boldsymbol{N}_C(r, x) = [N_C(r_1, x_1), \ldots, N_C(r_{n_r}, x_{n_x})]^T$ represents the collection response and $\boldsymbol{N}_L(r, x) = [N_L(r_1, x_1), \ldots, N_L(r_{n_r}, x_{n_x})]^T$ represents one library response.

3.1.3. 3-dimensional spectrometer response analysis

Although the spectrometer responses appear to possess radial symmetry, small differences between individual detector responses at equal radial and axial positions may actually provide physical insight into the essential scattering physics involved in the process (e.g. preferential scattering angles for neutrons of particular energies, or room scatter contributions resulting in response asymmetries). To take full advantage of the response data collected, it may be beneficial to extend our analysis further to include all three physical dimensions of the problem. For this 3-dimensional response analysis, the MSND counts are not summed. Instead, each of the 128 MSNDs is considered as an individual data point on a 3-dimensional grid (shown as squares in Figs. 3.1(A) and 3.2(A) above, color-coded according to their relative neutron detection intensities). This method provides the most complete description of the spectrometer response, representing it as a function of x-, y-, and z-axial position within the spectrometer volume, $N(x, y, z)$. In this case, the Pearson product-moment cross-correlation coefficient takes the form

$$r_{C,L} = \frac{1}{n_x \cdot n_y \cdot n_z} \cdot \sum_{k=1}^{n_z} \sum_{j=1}^{n_y} \sum_{i=1}^{n_x} \frac{N_C\left(x_i, y_j, z_k\right) - \overline{\boldsymbol{N}_C\left(x, y, z\right)}}{\sigma_{\boldsymbol{N}_C(x,y,z)}} \cdot \frac{N_L\left(x_i, y_j, z_k\right) - \overline{\boldsymbol{N}_L\left(x, y, z\right)}}{\sigma_{\boldsymbol{N}_L(x,y,z)}}, \tag{3.6}$$

where $\boldsymbol{N}_C(x, y, z) = [N_C(x_1, y_1, z_1), \ldots, N_C(x_{n_x}, y_{n_y}, z_{n_z})]^T$ represents the collection response and $\boldsymbol{N}_L(x, y, z) = [N_L(x_1, y_1, z_1), \ldots, N_L(x_{n_x}, y_{n_y}, z_{n_z})]^T$ represents one library response.

3.2. 6C software implementation

The library name and 1, 2, and 3-dimensional coefficients of determination (r^2) are displayed and updated in real time on the 6C spectrometer's user interface for the top 10 most correlated libraries (10 libraries, 30 r^2 values total shown) in descending order, and may be sorted by 1-D, 2-D, or 3-D coefficient at the operator's discretion (see Fig. 3.3, BOTTOM). In addition to this sorted table of values, the operator may also choose to view a real-time-updating coefficient of determination vs. time plot for the top 3 most correlated libraries, providing further insight into the neutron source identification decision as the collected data accumulates (Fig. 3.3, TOP).

3.3. Empirical analysis of Pearson cross-correlation methods

3.3.1. Experimental setup

To test and compare the efficacy of the 1-, 2-, and 3-dimensional Pearson cross-correlation methodologies with the 6C spectrometer, an experiment was conducted in the same 20-ft. × 30-ft. × 11-ft. room described in Section 2.3.1 (concrete walls and floor), in which a 5-min measurement was taken at a 5.0-m standoff distance from a bare 1.5×10^5-n/s ^{252}Cf source, at the reference angular orientation, 0° (i.e., such that the instrument's front circular face was directed toward the neutron source). Throughout the 5-min data collection, the three methods outlined in this section were applied once every second, and the time-dependent results were stored for subsequent analysis. Each time the methods were applied, the accumulated measurement data was compared to the entire pre-generated library of neutron source types and shielded configurations described in the beginning of Section 3.

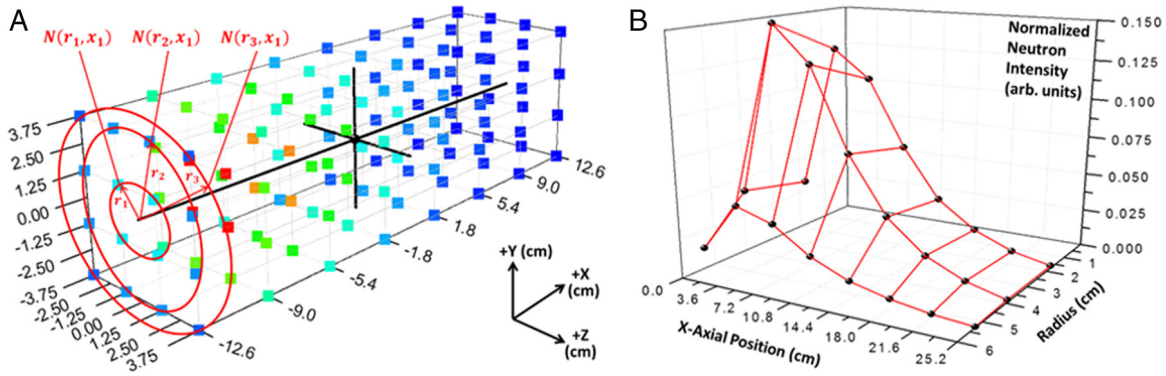

Fig. 3.2. (A) Example of a 2-dimensional cross-correlation data grouping applied to a simulated 6C spectrometer response to a bare ^{252}Cf neutron source, showing the three radial groupings for MSNDs located at $x_1 = -12.6$ cm in the defined 3-dimensional coordinate system. (B) Surface plot of the grouped 2-dimensional spectrometer response, showing normalized neutron detection intensity (arbitrary units) as a function of x-axial position (in cm) and radial position (in cm) in the coordinate system defined in Figure A, resulting from application of Eq. (3.4) (black circles with red linear interpolation lines). (For interpretation of the references to color in this figure legend, the reader is referred to the web version of this article.)

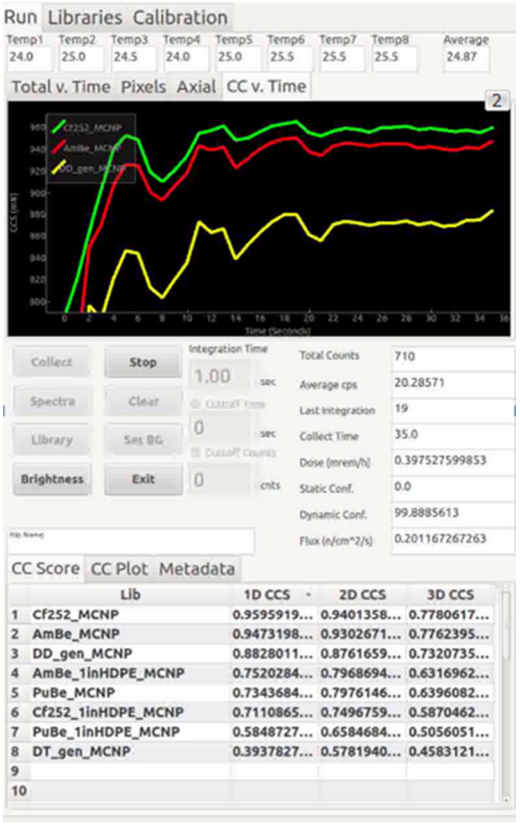

Fig. 3.3. Screen shot from the 6C spectrometer software taken during an empirical laboratory test at a 5.0-m standoff distance from a bare 1.5×10^5-n/s ^{252}Cf neutron source (discussed in Section 3.3), showing a correct source identification decision 35 s into the data collection. (TOP) Real-time-updating r^2 value vs. time plot for the top three most correlated source response libraries. (BOTTOM) Real-time-updating 1-D, 2-D, and 3-D r^2 value table for the top ten most correlated source response libraries (for illustrative purposes, only eight source libraries shown; sorted according to 1-D r^2 value, in descending order).

Only eight of these library responses will be discussed in the following section for illustrative purposes: (1) bare ^{252}Cf (the "true" source type in this experiment, [7,8]), (2) bare AmBe [7,8], (3) bare PuBe [7,11], (4) D–D fusion neutron generator (deuterium source–deuterium target, ~2.5 MeV), (5) D–T fusion neutron generator (deuterium source–tritium target, ~14.1 MeV), (6) ^{252}Cf enclosed in a 1 in. sphere of high density polyethylene (HDPE), (7) AmBe enclosed in a 1 in. sphere of HDPE, and (8) PuBe enclosed in a 1 in. sphere of HDPE. Each of these library responses were generated via MCNP6 simulation, disregarding environmental scattering effects (i.e., no floor/ground, walls, ceiling, etc. were included in the simulations). Note: although results will only be shown for the aforementioned eight library responses, the three most correlated responses in the entire pre-generated library are represented (bare ^{252}Cf, bare AmBe, and D–D generator); the other five library responses were chosen to illustrate additional (α, n) and fusion generator source types, and to compare lightly-shielded variants.

3.3.2. *Empirical results*

The results obtained from this 5-min measurement (Fig. 3.4(A)) show that the correct neutron source, bare ^{252}Cf, was identified using each of the three methods discussed in this section. In fact, the screen shot from the instrument's software (Fig. 3.3), taken 35 s into this measurement (710 total instrument counts), shows that the correct source was already identified at this time using each method.

When assessing the results in Fig. 3.4(A), due to the magnitude of the r^2 values, one may incorrectly conclude that the 1-dimensional correlation analysis outperformed the 2-dimensional analysis, and that the 2-dimensional analysis outperformed the 3-dimensional analysis. To more accurately characterize and compare the performance of each method, a confidence in each identification decision will be defined as the statistical certainty that the highest r^2 value obtained (r_1^2) is truly greater than the second highest r^2 value (r_2^2), or equivalently, the statistical certainty that the difference between the highest r^2 value and the second highest r^2 value (Δr^2) is truly greater than zero (for this test, Δr^2 values for bare ^{252}Cf and bare AmBe are shown in Fig. 3.4(B) for each method).

$$r_1^2 > r_2^2 \iff \Delta r^2 \equiv r_1^2 - r_2^2 > 0. \tag{3.7}$$

Basing this confidence upon only the highest two r^2 values can be understood intuitively. If your results show that $r_1^2 > r_2^2 > r_3^2 > \cdots > r_n^2$, and you are 98% confident that r_1^2 is truly greater than r_2^2, than you are more than 98% confident that r_1^2 is truly greater than r_3^2, r_4^2, …, and r_n^2. Since Eqs. (3.2)–(3.6), directly depend upon the counts obtained from each thermal neutron detector in the instrument, standard counting statistics and propagation of uncertainties can be applied to determine this statistical significance value (detailed description of this confidence metric and its derivation are outside the scope of this work; the metric was derived, in part, from concepts outlined in [12,13], and [14]). Although the ^{252}Cf source was correctly identified 35 s into this measurement (Fig. 3.3), the confidences in the source identification decision, as defined here, were only 76.75%, 65.55%, and 54.07% for the 1-, 2-, and 3-dimensional methods, respectively, at this time. All three of these confidence values grew steadily as counts accumulated over time, but the confidence for the 3-dimensional analysis grew at the highest rate, the 2-dimensional confidence grew at a moderate rate, and

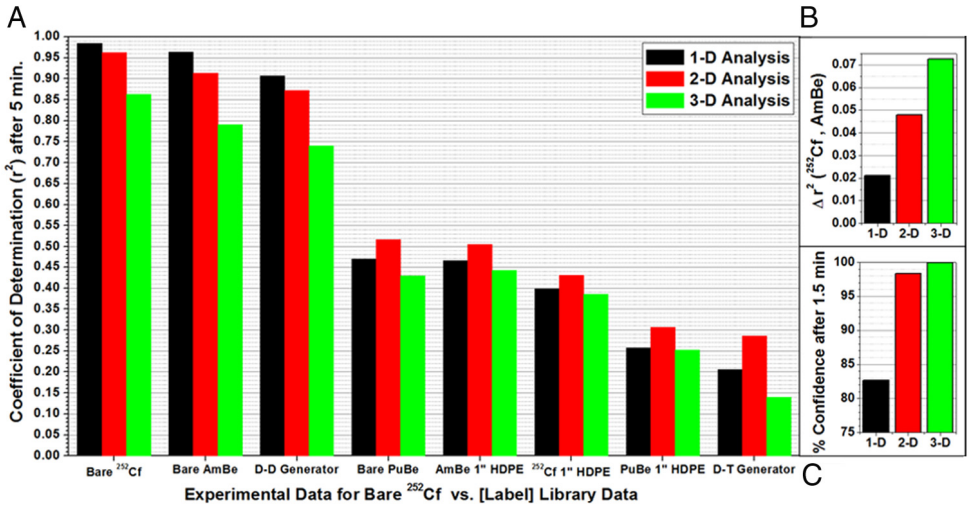

Fig. 3.4. (A) Summary plot of empirical results from a 5-min 6C spectrometer measurement with a bare 1.5×10^5-n/s ^{252}Cf spontaneous fission neutron source at a 5.0-m standoff distance, showing r^2 values obtained from 1-, 2-, and 3-dimensional Pearson correlation analysis techniques applied to experimentally-measured data and 8 library source types. (B) Plot of Δr^2 values for bare ^{252}Cf and bare AmBe vs. method. (C) Plot of % confidence in identification of bare ^{252}Cf after 1.5 min vs. method.

the 1-dimensional confidence grew at the lowest rate. Fig. 3.4(C) shows that the confidence values 1.5 min into the measurement were 82.67%, 98.38%, and 99.94% for the 1-, 2-, and 3-dimensional methods, respectively. By the end of the 5-min measurement, all three methods were successful in correctly identifying the source with >99.9% confidence; however, these results show that increasing the spatial dimensionality of the correlation analysis described in this section allows for a greater source identification confidence in less time.

4. Extension of 2-D & 3-D Pearson cross-correlation methods: simultaneous neutron source localization and identification

As mentioned in Section 3, the current implementation of the 1-D, 2-D, and 3-D Pearson correlation methodologies require the user to orient the 6C spectrometer such that its front circular face is directed toward the neutron source of interest prior to starting the source identification data collection. In an effort to eliminate the necessity of this prerequisite, an extension of the 2-D and 3-D Pearson cross-correlation techniques discussed in the previous section was conceived to allow for neutron source identification to be performed at any arbitrary source-to-spectrometer angular orientation. By construction, this methodological extension not only eliminates the instrument reorientation prerequisite for neutron source identification, it also may provide a means to determine the location and identity of a neutron source simultaneously. Prior to discussing this extension in detail, it is necessary to introduce an alternative 2-dimensional spectrometer response data grouping.

4.1. Alternative 2-dimensional spectrometer response analysis

While the 3-dimensional method extension is consistent with the data grouping discussed in Section 3.1.3 above, the 2-dimensional method extension requires an alternative data grouping to the one introduced in Section 3.1.2. As discussed in Section 2.1, the 6C spectrometer's response in the vertical dimension is much more sensitive to variations in environmental scattering conditions than its horizontal-planar components. To accommodate this known shortcoming, the counts from each vertical column of MSNDs in the instrument are summed for the alternative 2-D response analysis, providing the spectrometer response as a function of x-axial and z-axial position in the horizontal plane (Fig. 4.1), with each of the 32 data points given by

$$N\left(x_i, z_k\right) = \sum_{j=1}^{n_y} N\left(x_i, y_j, z_k\right). \tag{4.1}$$

4.2. 2-D and 3-D Pearson cross-correlation method extension

Recall, from Section 3.1, that the currently implemented method for neutron source identification allows for a priori source information to be uploaded in the form of neutron energy spectra, which are subsequently normalized, rebinned, and "folded into" (i.e., multiplied by) the instrument's response matrix (pre-loaded in the 6C software, for front-face orientation) to generate expected response libraries for the new source type(s). This functionality serves as the basis for the methodological extension discussed here, in which response matrices are, instead, preloaded in the instrument's software for source-to-spectrometer angular orientations of $\theta = 0°$ to 355° in 5° increments in the horizontal x–z-plane (72 response matrices total, although the 5° angular increment chosen for this study is relatively arbitrary). For each of these 72 angular orientations, the angular response matrix is generated through a set of MCNP simulations for 128 discretely-binned neutron energy ranges, E_l, which span the range [1.0E−9 MeV, 100 MeV] in even logarithmic decrements (i.e., the quantity $\log_{10}\left(\max\left(E_l\right)/\min\left(E_l\right)\right)$ is equal for all 128 binned ranges, E_l, and $\bigcup_l E_l = \left[\min\left(E_1\right), \max\left(E_{128}\right)\right]$ = [1.0E − 9 MeV, 100 MeV]). The 128 × 128 response matrix (one row for each MSND in the instrument, one column for each discretely-binned energy range) for each angular orientation, θ, is then calculated as

$$\boldsymbol{R}^{\theta}_{128\times128}(x,y,z,E) = \begin{bmatrix} P\left(N\left(x_1,y_1,z_1\right)|E_1,\theta\right) & \cdots & P\left(N\left(x_1,y_1,z_1\right)|E_{128},\theta\right) \\ \vdots & \ddots & \vdots \\ P\left(N\left(x_8,y_4,z_4\right)|E_1,\theta\right) & \cdots & P\left(N\left(x_8,y_4,z_4\right)|E_{128},\theta\right) \end{bmatrix} \cdot A(\theta), \tag{4.2}$$

$$A(\theta) = D\cdot L\cdot\sin\theta + \frac{\pi}{4}\cdot D^2\cdot\cos\theta,$$

where D and L are the diameter and length (in cm), respectively, of the active portion of the instrument (i.e., the cylindrical HDPE moderating volume), $A(\theta)$ is the cross-sectional area (in cm^2) of the active portion of the instrument for which the normal vector is at angular orientation θ (examples shown in Fig. 4.2 for the 6C spectrometer: $L \cong 30.48$ cm and $D = 15.24$ cm), and each $P\left(N\left(x_i,y_j,z_k\right)|E_l,\theta\right)$ represents the conditional probability that a neutron – incident upon the active portion of the instrument – will be detected by the MSND located at $\left(x_i,y_j,z_k\right)$, given that the incident energy of the neutron is in the discrete range E_l and that the neutron was emitted from a source located at angular orientation θ relative to the instrument.

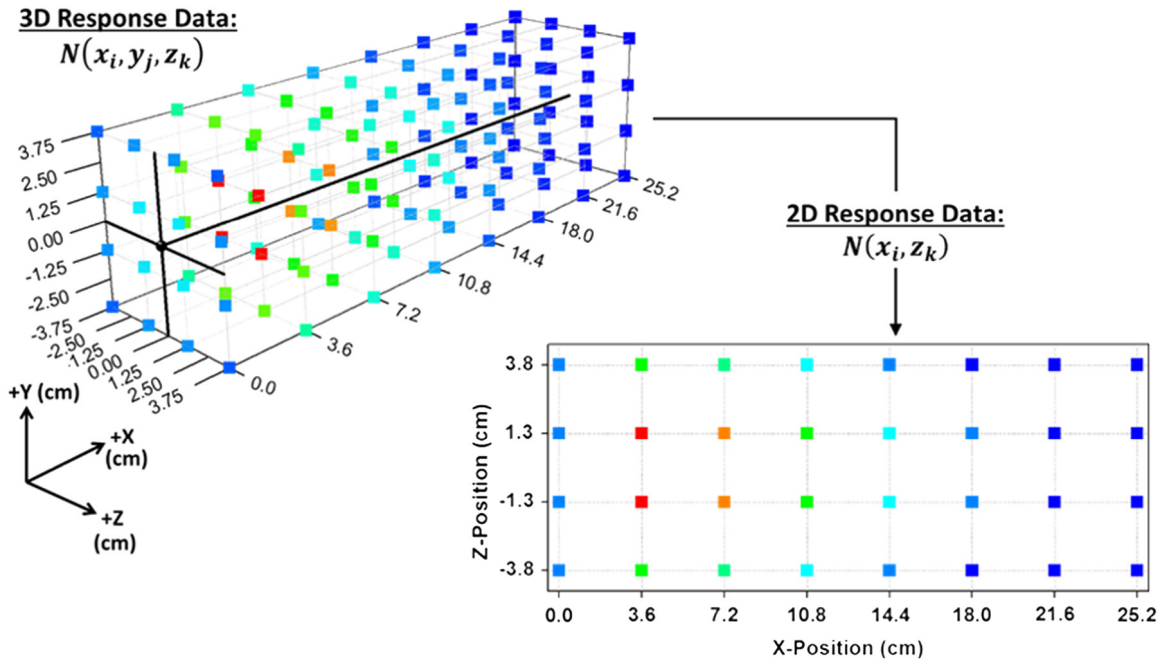

Fig. 4.1. Example of the alternative 2-dimensional cross-correlation data grouping applied to a simulated 6C spectrometer response to a bare ^{252}Cf neutron source.

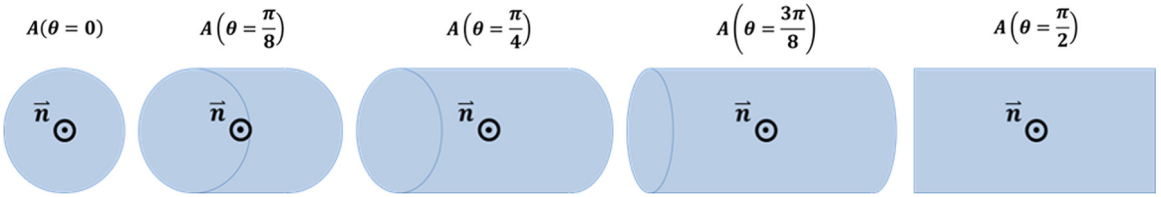

Fig. 4.2. Illustration of 6C spectrometer cross-sectional areas, $A(\theta)$ in Eq. (4.2), (all blue area) for source-to-spectrometer angular orientations of $\theta = 0$ to $\pi/2$ radians (0° to 90°) in $\pi/8$ radian (22.5°) increments (left to right). For each angular orientation shown, the vector normal to the surface, $\vec{n}$, is in the direction of the neutron source (directly out of the page in each illustration). Darker blue edge lines added to aid visualization of each moderating cylinder orientation.

With the response matrices calculated according to Eq. (4.2), and preloaded in the instrument's software, 3-dimensional library responses can be generated for each angular orientation (θ = 0° to 355° in 5° increments) for any neutron source of interest by rebinning its neutron energy spectrum to match the response matrix binning structure, and multiplying it by each angular response matrix. This can be shown using the following linear model for the expected 3-dimensional library response to neutron source L at source-to-spectrometer angular orientation θ:

$$\boldsymbol{N}_L^{\theta}(x,y,z) = \boldsymbol{R}^{\theta}(x,y,z,E)\cdot\boldsymbol{\Phi}_L(E) = \left(\begin{bmatrix} P\left(N\left(x_1,y_1,z_1\right)|E_1,\theta\right) & \cdots & P\left(N\left(x_1,y_1,z_1\right)|E_{128},\theta\right) \\ \vdots & \ddots & \vdots \\ P\left(N\left(x_8,y_4,z_4\right)|E_1,\theta\right) & \cdots & P\left(N\left(x_8,y_4,z_4\right)|E_{128},\theta\right) \end{bmatrix} \cdot A(\theta)\right)\cdot\left(\begin{bmatrix} P_L(E_1) \\ \vdots \\ P_L(E_{128}) \end{bmatrix}\cdot\left|\boldsymbol{\Phi}_L(E)\right|\right), \tag{4.3}$$

where $\boldsymbol{\Phi}_L(E)$ is the local (i.e., incident upon the active portion of the instrument), discretized, energy-dependent neutron fluence from source L (in ${}_0^1n/\mathrm{cm}^2$), $\left|\boldsymbol{\Phi}_L(E)\right|$ is its magnitude (in the same units), and $\left[P_L(E_1)\cdots P_L(E_{128})\right]^T$ is the rebinned energy spectrum of neutron source L (i.e., each $P_L(E_l)$ represents the probability that the energy of a neutron emitted from source L will be in the discrete range E_l). Since the Pearson product-moment cross-correlation coefficient, which will be utilized for this analysis, is invariant to linear combinations, and both the cross sectional area, $A(\theta)$, and the magnitude of the local neutron fluence, $\left|\boldsymbol{\Phi}_L(E)\right|$ will be constants for any static measurement (i.e., stationary source and stationary instrument), these two terms of Eq. (4.3) may be ignored (i.e., set to unity) without losing any information pertinent to the source identification analysis, such that

$$\boldsymbol{N}_L^{\theta}(x,y,z) = \begin{bmatrix} P\left(N\left(x_1,y_1,z_1\right)|E_1,\theta\right) & \cdots & P\left(N\left(x_1,y_1,z_1\right)|E_{128},\theta\right) \\ \vdots & \ddots & \vdots \\ P\left(N\left(x_8,y_4,z_4\right)|E_1,\theta\right) & \cdots & P\left(N\left(x_8,y_4,z_4\right)|E_{128},\theta\right) \end{bmatrix} \cdot \begin{bmatrix} P_L(E_1) \\ \vdots \\ P_L(E_{128}) \end{bmatrix}. \tag{4.4}$$

Operationally, a large list of source spectra $\left(\boldsymbol{P}_{L_1}(E),\ldots,\boldsymbol{P}_{L_M}(E)\right)$ is chosen to include as many neutron source types and/or shielded variants as necessary for a given application. Each of these source spectra are then multiplied by each of the 72 angular response matrices (Eq. (4.4)) to yield a set of 3-dimensional library spectrometer responses $\boldsymbol{N}_L^{\theta}(x,y,z)$, for θ = 0°, 5°, …, 355°, and $L = L_1, L_2, \ldots, L_M$ ($72\cdot M$ libraries total, where M is the number of source types and/or shielded variants of interest). These library responses are then grouped according to Eq. (4.1) for subsequent use in the 2-dimensional analysis,

$$N_L^{\theta}(x_i,z_k) = \sum_{j=1}^{n_y} N_L^{\theta}(x_i,y_j,z_k). \tag{4.5}$$

Once the desired 2-D and 3-D response libraries have been selected and generated, data collection may be initiated (without having to reorient the instrument). During data collection, the live response data is grouped for 2- and 3-dimensional real-time comparison to each individual library response using the Pearson cross-correlation method discussed in Section 3. In this case, the 3-D correlation coefficient is of the form

$$r_{C,L} = \frac{1}{8\cdot 4\cdot 4}\cdot\sum_{k=1}^{4}\sum_{j=1}^{4}\sum_{i=1}^{8}\frac{N_C\left(x_i,y_j,z_k\right)-\overline{\boldsymbol{N}_C\left(x,y,z\right)}}{\sigma_{\boldsymbol{N}_C(x,y,z)}}\cdot\frac{N_L^{\theta}\left(x_i,y_j,z_k\right)-\overline{\boldsymbol{N}_L^{\theta}\left(x,y,z\right)}}{\sigma_{\boldsymbol{N}_L^{\theta}(x,y,z)}}, \tag{4.6}$$

where $\boldsymbol{N}_C(x,y,z) = [N_C(x_1,y_1,z_1),\ldots,N_C(x_8,y_4,z_4)]$ represents the collection response and $\boldsymbol{N}_L^{\theta}(x,y,z) = [N_L^{\theta}(x_1,y_1,z_1),\ldots,N_L^{\theta}(x_8,y_4,z_4)]$ represents one library response, and the 2-D correlation coefficient is of the form

$$r_{C,L} = \frac{1}{4\cdot 8}\cdot\sum_{k=1}^{4}\sum_{i=1}^{8}\frac{N_C\left(x_i,z_k\right)-\overline{\boldsymbol{N}_C\left(x,z\right)}}{\sigma_{\boldsymbol{N}_C(x,z)}}\cdot\frac{N_L^{\theta}\left(x_i,z_k\right)-\overline{\boldsymbol{N}_L^{\theta}\left(x,z\right)}}{\sigma_{\boldsymbol{N}_L^{\theta}(x,z)}}, \tag{4.7}$$

where $\boldsymbol{N}_C(x,z) = [N_C(x_1,z_1),\ldots,N_C(x_8,z_4)]$ represents the collection response and $\boldsymbol{N}_L^{\theta}(x,z) = [N_L^{\theta}(x_1,z_1),\ldots,N_L^{\theta}(x_8,z_4)]$ represents one library response.

Similar to the Pearson correlation analysis discussed in Section 3, the 2-D and/or 3-D library response that is most positively correlated to the live response, according to the value of $r_{C,L}^2$, is then chosen as the most likely source of the incident neutron radiation (of the source libraries uploaded). Here, however, the most positively correlated response library $\boldsymbol{N}_L^{\theta}$ corresponds to both a particular source-to-spectrometer relative angular orientation in the horizontal x–z-plane, θ, and a particular source type, L. Hence, without being required to reorient the instrument, the user is provided with neutron source location and identification information simultaneously. Furthermore, since the source libraries are generated and loaded prior to data collection (Eqs. (4.2)–(4.5)), and the cross-correlation calculations are computationally inexpensive (Eqs. (4.6) and (4.7)), this information can be displayed to the user in real time updates as data is being collected. In preliminary simulation tests, in which 6 source types were simulated in horizontal-planar angular orientations of 0° to 355° in 5° increments ($6\cdot(360/5) = 432$ simulations total), the correct source type was identified in all simulated trials, with average angular location errors of ±2.5° for the 2-dimensional method extension (i.e., a 64.29% improvement to the NRV method results) and ±5° for the 3-dimensional method extension (i.e., a 28.57% improvement to the NRV method results). While these initial theoretical results are very promising, empirical tests of these methodological extensions have yet to be conducted, and will be the subject of future work.

5. Post-hoc improvement to the NRV method: NRV-Poly method

This algorithmic improvement to the neutron response vectorization (NRV) method, called the NRV-Poly method, is based on thoroughly characterizing the accuracy of the NRV method as a function of true source-to-spectrometer angular orientation, then making post-hoc adjustments to NRV method results based upon this characterization. Thus, Section 5.1 will discuss one way in which the accuracy of the NRV method (applied to 6C spectrometer measurements) can be characterized analytically, and Section 5.2 will discuss how this characterization can be utilized to make post-hoc adjustments to NRV method results, improving the accuracy and consistency of horizontal-planar angular orientation determinations.

5.1. NRV-Poly method: continuous polynomial functional fit characterization

To characterize the theoretical accuracy of the existing NRV method as a function of true source-to-spectrometer angular orientation, the method (without the geometric asymmetry correction step, i.e., skipping Eq. (2.2)) was applied to simulated 6C spectrometer responses to a bare ^{252}Cf neutron source at angular orientations ranging from 0° to 355° in 5° increments. The difference between the angular orientation obtained through application of the NRV method and the true (simulated) angular orientation (i.e. the NRV method errors) were then plotted as a function of the true angular orientation (red and blue circles in Fig. 5.1). These data points were then separated, according to the simulated true angle, into two overlapping data sets – data set A from −15° (345°) to 195° and data set B from 165° to 375° (15°) – and a 13th order polynomial curve fit (found to provide the best r^2 value fit to the data without overfitting) was applied to each data set using the NumPy "polyfit" Python routine (least-squares polynomial fit, [15]), providing values for the 28 coefficients a_i and b_i in Eqs. (5.1) and (5.2) below.

$$\theta_{\mathrm{NRV}}^{(A)} - \theta = a_0 + a_1\cdot\theta + a_2\cdot\theta^2 + \cdots + a_{13}\cdot\theta^{13} \quad \text{and} \tag{5.1}$$

$$\theta_{\mathrm{NRV}}^{(B)} - \theta = b_0 + b_1\cdot\theta + b_2\cdot\theta^2 + \cdots + b_{13}\cdot\theta^{13}, \tag{5.2}$$

where θ_{NRV} and θ represent the NRV measured angle and true angle (in degrees), respectively, with Eq. (5.1) corresponding to data set A and Eq. (5.2) corresponding to data set B.

With the coefficients a_i and b_i determined, simple algebraic manipulation of Eqs. (5.1) and (5.2) yields the desired NRV method characterization: two analytical functions describing the behavior of results obtained through application of the NRV method as a function true source-to-spectrometer angular orientation for data sets A and B (Eqs. (5.3) and (5.4) below, represented as red and blue lines in Fig. 5.2, respectively).

$$\theta_{\mathrm{NRV}}^{(A)} = a_0 + \left(a_1+1\right)\cdot\theta + a_2\cdot\theta^2 + \cdots + a_{13}\cdot\theta^{13} \quad \text{and} \tag{5.3}$$

$$\theta_{\mathrm{NRV}}^{(B)} = b_0 + \left(b_1+1\right)\cdot\theta + b_2\cdot\theta^2 + \cdots + b_{13}\cdot\theta^{13}. \tag{5.4}$$

5.2. NRV-Poly method: post-hoc adjustment

When analyzing live measurement data, the NRV-Poly method first uses the "base" NRV method to obtain an initial "NRV measured angle", θ_{NRV}. If θ_{NRV} is in the range $[0°, 180°)$, it is substituted for $\theta_{\mathrm{NRV}}^{(A)}$ in Eq. (5.3), and if θ_{NRV} is in the range $[180°, 360°)$, it is substituted for $\theta_{\mathrm{NRV}}^{(B)}$ in Eq. (5.4). The resulting equation (Eq. (5.3) or (5.4) with θ_{NRV} substituted) is then solved for θ by finding the roots of the corresponding algebraically manipulated equation,

$$\begin{cases} 0 = \left(a_0-\theta_{\mathrm{NRV}}\right) + \left(a_1+1\right)\cdot\theta + a_2\cdot\theta^2 + \cdots + a_{13}\cdot\theta^{13}, \\ \quad \theta_{\mathrm{NRV}} \in \left[0^{\mathrm{o}}, 180^{\mathrm{o}}\right) & \text{(a)} \\ 0 = \left(b_0-\theta_{\mathrm{NRV}}\right) + \left(b_1+1\right)\cdot\theta + b_2\cdot\theta^2 + \cdots + b_{13}\cdot\theta^{13}, \\ \quad \theta_{\mathrm{NRV}} \in \left[180^{\mathrm{o}}, 360^{\mathrm{o}}\right) & \text{(b)} \end{cases} \tag{5.5}$$

using the NumPy "roots" Python routine [15,16]. Since Eqs. (5.5)(a) and (5.5)(b) are both 13th order polynomials, the NumPy roots routine will always return a list of exactly 13 possible solutions for θ. Recognizing that the desired solution should always be real-valued (in this case), the list of possible solutions is then narrowed down by eliminating any solutions with non-zero imaginary components. From this smaller list of possible real-valued solutions, the solution that is closest to the NRV measured angle, θ_{NRV}, (modulo 360) is chosen as the new "NRV-Poly measured angle". Both the NRV measured angle and the NRV-Poly measured angle are calculated and updated once every software iteration (i.e. every user-defined time step, in seconds) and the results are saved for further analysis. Additionally, two method comparison

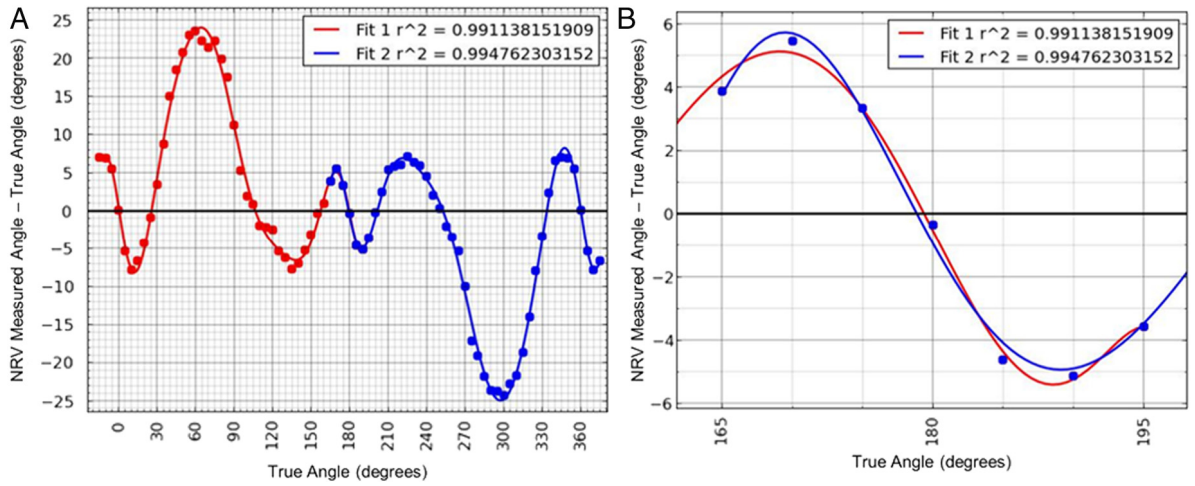

Fig. 5.1. (A) Plot of simulated results (circles) and 13th order polynomial curve fits (solid lines) for data sets A (red) and B (blue), showing NRV measured angle–True Angle vs. True Angle with r^2 values for each fit given in the legend. (B) Magnified view of the 30° overlapping region surrounding True Angle = 180°. (For interpretation of the references to color in this figure legend, the reader is referred to the web version of this article.)

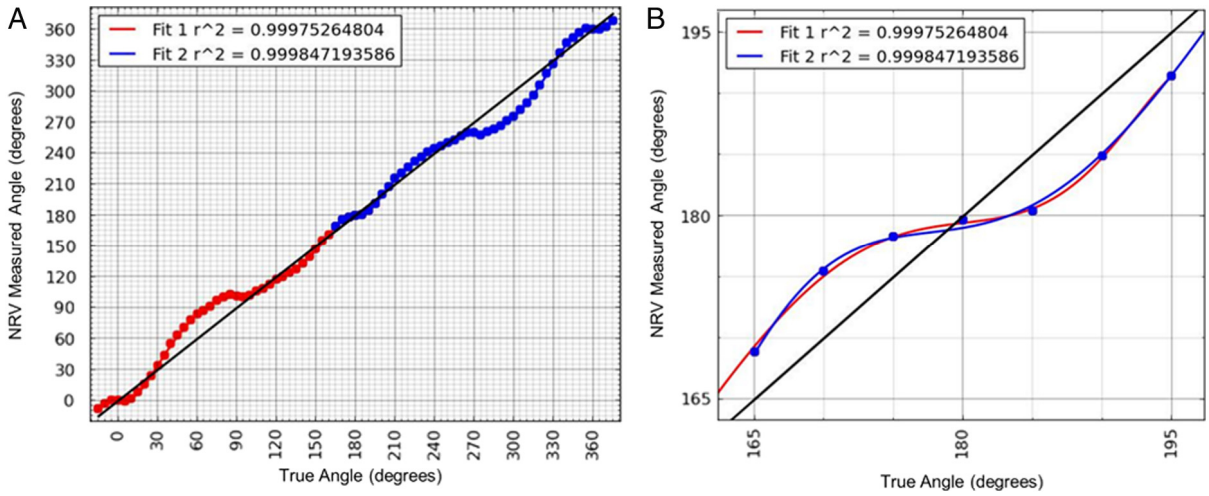

Fig. 5.2. (A) Plot of simulated results (circles) and 13th order polynomial curve fits (solid lines) for data sets A (red) and B (blue), showing NRV measured angle vs. True Angle with r^2 values for each fit given in the legend. (B) Magnified view of the 30° overlapping region surrounding True Angle = 180°. (For interpretation of the references to color in this figure legend, the reader is referred to the web version of this article.)

summary plots are created and saved at the completion of each experiment. Fig. 5.3, shows example output plots from a simulation in which 5809 total neutrons were detected from a bare ^{252}Cf source at a 300° source-to-spectrometer (true) angular orientation.

As can be seen from the simulated test results in Fig. 5.3, the NRV-Poly method appears to be a very promising improvement to the existing NRV method, decreasing the angular error by ±24.75° in this case. However, like the Pearson correlation method extensions discussed in Section 4, empirical analysis will be necessary to determine the true efficacy of the NRV-poly method, and will be the subject of future work.

6. Conclusions and future work

Two "core" algorithmic methodologies were presented for determining the relative location and the identity of sources of neutron radiation with a volumetrically-sensitive moderating-type neutron spectrometer. Two extensions of – and potential improvements to – these core methodologies were then proposed. The Neutron Response Vectorization (NRV) Method was introduced as the core methodology for determining the location of a neutron source relative to an instrument. It was shown that the NRV method, when applied to empirical 6C spectrometer measurements, provided an accurate determination of the relative horizontal-planar angular location of a bare ^{252}Cf neutron source, in a high-scattering environment, with an average angular error of ±7°. Pearson product-moment cross-correlation spatial response analysis techniques (in 1, 2, and 3 spatial dimensions) were then introduced as the core methodologies for determining the most probable identity of a neutron source. It was shown that each of these spatial response analysis techniques, when applied to empirical 6C spectrometer measurements, were capable of correctly identifying a bare ^{252}Cf neutron source in less than one minute, and that increasing the spatial dimensionality of the correlation analysis allows for a greater source identification confidence in less time. A methodological extension of the 2- and 3-dimensional Pearson cross-correlation techniques was then proposed to simultaneously determine the identity of a neutron source and its relative angular location in the horizontal plane. In a set of 432 simulation tests, the correct source type was identified in all trials, with average angular location errors of ±2.5° for the 2-dimensional method extension (i.e., a 64.29% improvement to the NRV method results) and ±5° for the 3-dimensional method extension (i.e., a 28.57% improvement to the NRV method results). Lastly, a post-hoc improvement to the NRV method, employing a continuous polynomial fit characterization, was proposed

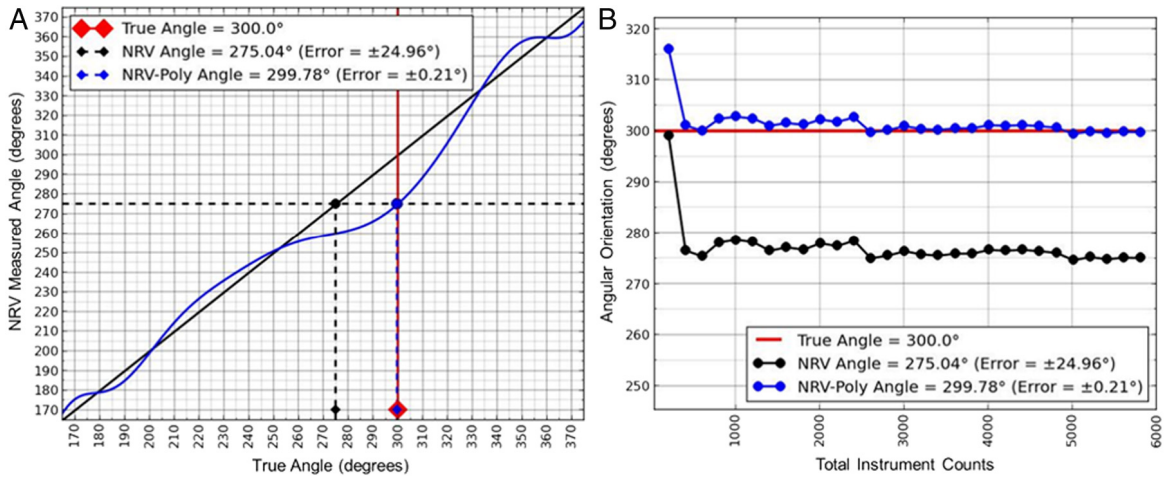

Fig. 5.3. Example output plots from a simulation in which 5809 total neutrons were detected from a bare ^{252}Cf source at a 300° source-to-spectrometer angular orientation. (A) Plot of NRV measured angle vs. true angle, showing final resultant angles (small diamonds and dotted lines) obtained from application of the NRV method (black) and the NRV-poly method (blue), with the polynomial curve fit (solid blue line), true angle (large red diamond and solid red line), and NRV measured angle = true angle line (solid black line) shown for reference. (B) Plot of resultant measured angular orientations using the NRV method (black) and the NRV-Poly method (blue) vs. total instrument counts for even time intervals throughout the example simulation (circles and solid linear interpolation lines), with the true simulated angle (solid red line) shown for reference. (For interpretation of the references to color in this figure legend, the reader is referred to the web version of this article.)

(the NRV-Poly method). In preliminary simulation testing, the NRV-Poly method was shown to be a very promising algorithmic improvement, decreasing the angular error from ±24.96° to ±0.21° (i.e., a 99.16% improvement) in the example discussed in Section 5.

Through extensive empirical testing on multiple volumetrically-sensitive moderating-type instruments, the core methodologies introduced in this work (i.e., the Pearson correlation spatial analysis techniques and the NRV method) have proven to be accurate and reliable for determining the identity and horizontal-planar location of sources of neutron radiation in a variety of operational environments; however, the methodological extensions introduced in this work could provide improved accuracy and reliability, as well as ease of instrument use. While the initial theoretical results are very promising, thorough empirical tests of the two methodological extensions discussed in Sections 4 and 5 have yet to be conducted, and will be the subject of future work. Additional future works will focus on extending the angular location methodologies discussed here to include the vertical dimension, providing a means to real-time neutron-based source imaging with a portable moderating-type instrument.

Acknowledgments

This work was funded by the Office of Naval Research, award nos. N00014-11-1-0157 and N00014-13-1-0402, and by the Defense Threat Reduction Agency, award no. HDTRA1-14-P-005.

References

[1] C.B. Hoshor, T.M. Oakes, E.R. Myers, B.J. Rogers, J.E. Currie, S.M. Young, J.A. Crow, P.R. Scott, W.H. Miller, S.L. Bellinger, D.S. McGregor, A.N. Caruso, A portable and wide energy range semiconductor-based neutron spectrometer, Nucl. Instrum. Methods Phys. Res. A 803 (2015) 68–81.

[2] Richard L. Bramblett, R.I. Ewing, T.W. Bonner, A new type of neutron spectrometer, Nucl. Instrum. Methods 9 (1) (1960) 1–12.

[3] Paul Goldhagen, An extended-range multisphere neutron spectrometer with high sensitivity and improved resolution, Nucl. Technol.: Radiat. Meas. Gen. Instrum. 175 (1) (2011) 81–88.

[4] A.O. Hanson, J.L. McKibben, A neutron detector having uniform sensitivity from 10 keV to 3 MeV, Phys. Rev. 72 (8) (1947) 673.

[5] Thomas M. Oakes, Modeling and Analysis of a Portable, Solid-State Neutron Detection System for Spectroscopic Applications, Doctor of Philosophy Dissertation, University of Missouri, Columbia, Missouri, 2012.

[6] J.K. Shultis, D.S. McGregor, Design and performance considerations for perforated semiconductor thermal-neutron detectors, Nucl. Instrum. Methods Phys. Res. Sect. A 606 (2009) 608–636.

[7] IAEA, Compendium of Neutron Spectra and Detector Responses for Radiation Protection Purposes. Technical Reports Series no. 403, Supplement to Technical Reports Series No. 318. Vienna, 2001.

[8] A.V. Alevra, H. Klein, K. Knauf, J. Wittstock, Neutron field spectrometry for radiation protection dosimetry purposes, Radiat. Prot. Dosim. 44 (1992) 223–226.

[9] Eliot R. Myers, Neutron Response Vectorization and Optimization of Moderating Neutron Spectrometers for Active Interrogation. Master of Science Thesis, University of Missouri-Kansas City, Kansas City, Missouri, 2015.

[10] Karl Pearson, Note on regression and inheritance in the case of two parents, Proc. R. Soc. Lond. 58 (1895) 240–242.

[11] R.V. Griffith, multi-technique characterization of neutron fields from moderated ^{252}Cf and ^{238}PuBe sources, in: National and International Standardization of Radiation Dosimetry (Proc. Symp. Atlanta, 1977), 2, IAEA, Vienna, 1978, pp. 167–188.

[12] Glenn F. Knoll, Radiation Detection and Measurement, John Wiley & Sons, 2010.

[13] Radiation Counting Statistics. Safety Support Series Volume 1, International Safety Research, ©2000–2013.

[14] François Lemay, Multichannel statistical analysis of low-level radioactivity in the presence of background counts, Health Phys. 103 (6) (2012) 770–779.

[15] Ivan Idris, NumPy Cookbook, Packt Publishing Ltd., 2015.

[16] R.A. Horn, C.R. Johnson, Matrix Analysis, Cambridge University Press, Cambridge, UK, 1999, pp. 146–147.